EFFECT OF ZINC ADDITION IN COPPER TO STRUCTURE, HARDNESS, CORROSION, AND ANTIBACTERIAL ACTIVITY

by Lisa Samura FTKE

Submission date: 03-Dec-2024 08:05PM (UTC+0700)
Submission ID: 2252552734
File name: JAETS_Lisa_Samura_Rev_19_11_2024.pdf (1.26M)
Word count: 6908
Character count: 36767

Journal of Applied Engineering and Technological Science
Vol xx(x) 201x :
xx-xx

EFFECT OF ZINC ADDITION IN COPPER TO STRUCTURE, HARDNESS, CORROSION, AND ANTIBACTERIAL ACTIVITY

Lisa Samura[1*], Mustamina Maulani[1], Cahaya Rosyidan[1], Kartika Fajarwati Hartono[1], Suryo Prakoso[1], Evi Ulina Margareta Situmorang[2], Daniel Edbert[3], Bambang Soegijono[4], Muhammad Yunan Hasbi[5], Ferry Budhi Susetyo[6]
Department of Petroleum Engineering, Universitas Trisakti, 11440, Indonesia[1]
Department of Physiology School of Medicine and Health Sciences, Atma Jaya Catholic University of Indonesia, 14440, Indonesia[2]
Department of Microbiology, Atma Jaya Catholic University of Indonesia, 14440, Indonesia[3]
PROUDTEK Lab., Department of Geoscience, Universitas Indonesia, 16424, Indonesia[4]
Research Center for Metallurgy – National Research and Innovation Agency, 15314, Indonesia[5]
Department of Mechanical Engineering, Universitas Negeri Jakarta, 13220, Indonesia[6]
lisa.samura@trisakti.ac.id

**Coresponding Author*

ABSTRACT
Brass (CuZn) is widely used today due to better mechanical, thermal, and chemical properties. The present research fabricated CuZn alloy by adding various Zn (6, 9, and 12 wt.%) to the Cu using gravity casting. Casts CuZn alloy by adding various Zn to the Cu to investigate optimum composition were resulting highest inhibited of bacterial activity. In addition, the structure, hardness, and electrochemical behavior of the alloy were also investigated using XRD, Vickers hardness, and potentiostat equipment. XRD confirmed that CuZn alloy has an alpha phase, and a FCC crystal structure. The rise of the Zn content in the alloy led to an increase in crystallite size, a decrease in the hardness and a shift to a more negative OCP potential at 1200 s measurement. Enhancing the Zn content to 9 wt.% in the alloy lead to decrease the corrosion rate. Moreover, 24-hour post-contact observation found that the sample places removed remained clear of bacteria. The Cu6Zn sample successfully inhibited the growth of Escherichia coli in the 3rd hour, while Staphylococcus aureus was 100 % reduced in the 7th hour. The Cu6Zn sample could be used as an alternative material for medical equipment in ambulances.
Keywords : *XRD, Vickers, Electrochemical measurement, Staphylococcus aureus, Escherichia coli*

1. Introduction

Brass (CuZn) is an alloy widely used in the national defense, oil and gas industries, and health because it has better mechanical properties, thermal conductivity, and corrosion resistance (Bhavsar & Bali, 2023; Wang et al., 2023; Widyastuti et al., 2023). CuZn alloys for medical equipment in transportation such as ambulances need to consider two parameters: corrosion resistance and antibacterial characteristics. Commonly NaCl media was used to investigate corrosion for ambulance equipment. This condition due to ambulance equipment commonly exposure from medical patients eccrine sweat and saline-infused (Baker & Wolfe, 2020; Tayyab et al., 2021). Furthermore, some studies found that after cleaning the ambulance, 35.37 % of bacterial contaminants were still seen (Syamsuir et al., 2023).

Viegas et al. found *Staphylococcus aureus* was detectable on firefighter's ambulance equipment (Viegas et al., 2021). *Staphylococcus aureus* is a type of bacteria that could cause skin disease and is hard to treat with traditional antibiotics. *Staphylococcus aureus* bacteria tend to have methicillin resistance. According to Tajik et al., 38.4 % of *Staphylococcus aureus* methicillin resistant was found in Tehran community (Tajik et al., 2020). Moreover, this bacteria also could contaminate orthopedic implants and cause serious infections (Pietrocola et al., 2022).

Several researchers were interested in investigating the corrosion behavior of CuZn alloy in NaCl medium (Abed & Dawood, 2022; Chen et al., 2024; Gao et al., 2021; Yin et al., 2021). Abed and Dawood investigated the corrosion behavior of Cu40Zn alloy in 3.5% NaCl and found a corrosion rate of around 0.037 mmpy (Abed & Dawood, 2022). Yin et al. investigated the corrosion behavior of Cu alloy in NaCl medium were immersed in different times. More time is immersed, resulting in more corrosion resistance of Cu (Yin et al., 2021). Chen et al. investigated Cu alloy in NaCl medium and found Cu potential around -0.305 V vs SCE and Zn potential around -1.165 V vs SCE (Chen et al., 2024). Gao et al. found that a reduction in thickness (50 to 60 %) of CuZn using cold rolling resulted in a significant decrease in corrosion current from 4.824 to 1.804 μA/cm^2 (investigating in 3.5 % NaCl) (Gao et al., 2021). Moreover, aluminum (Al) alloy widely used in transportation sector such as ambulance (Blanco et al., 2022; Vandersluis et al., 2020). Liu et al. have found Al alloy corrosion current between 4.868-5.251 A/cm^2 in a 3.5% NaCl medium (Liu et al., 2020). Comparing the studies of Liu et al. and Gao et al., Al alloy has a higher corrosion current than CuZn (Gao et al., 2021; Liu et al., 2020). Corrosion current significantly influences the corrosion rate, and a rise in the corrosion current would enhance the corrosion rate.

Recently, researchers have been interested in investigating CuZn alloy for medical applications (Azizian et al., 2024; Riaz et al., 2024; Sabbouh et al., 2023). Azizian et al. investigated CuZn alloys microstructure, mechanical properties and cytotoxicity for cardiovascular applications (Azizian et al., 2024). Riaz et al. investigated the structural and biological properties of CuZn alloy for orthopedic applications (Riaz et al., 2024). Moreover, Sabbouh et al. did the sonification of CuZn in an alkali solution to enhance the antibacterial inhibition zone (Sabbouh et al., 2023). Moreover, Syamsuir et al. have investigated the antibacterial activity of *Staphylococcus aureus* by presenting a Cu layer for ambulance equipment (Syamsuir et al., 2023).

The killing mechanism of bacterial activity inseparable from the ions released by the alloy (Qu et al., 2020). Cu^{2+} ions could be adsorbed on the cytoplasmic membrane surfaces, then penetrate the bacteria, react with sulfhydryl groups, and cause the cell to die (Zeng et al., 2022). The released Zn^{2+} ions could penetrate the cell membrane and cause cell death (Du et al., 2021). Zhang et al. have stated that Cu^{2+} and Zn^{2+} ions could act as antibacterial agents and inhibit *Staphylococcus aureus* growth (Zhang et al., 2021).

According to the literature review, research on CuZn alloys with Zn compositions in the range of 6–12 wt.% for medical transportation purposes has not been thoroughly investigated. As mentioned above, the killing mechanism of bacterial activity depend on Cu and Zn ions. CuZn alloy can transform into Cu and Zn ions. Therefore, the present research casts CuZn alloy by adding various Zn to the Cu to investigate optimum composition, resulting in a higher killing mechanism of bacterial activity. Moreover, different alloy compositions would result in different electrochemical behavior and mechanical properties. The present study investigated structure, hardness, electrochemical behavior, and antibacterial activity using X-ray diffraction (XRD), Vickers hardness equipment, potentiostat, and digital camera.

2. Literature Review

Many techniques are used to make CuZn alloys, including gravity and investment casting (Hendrawan et al., 2021; Ziat et al., 2020). Gravity casting is simple, inexpensive, and can rapidly fill complex geometry (Huang et al., 2024; Nuryadi et al., 2020). Moreover, in the fabrication of CuZn alloys, one thing needs to be considered to produce specific properties, namely alloy composition. Researchers focused on adding various Zn compositions onto Cu for different purposes. Strzępek et al. investigated the mechanical properties of Cu and alpha brass (Cu2.5Zn and Cu6.5Zn) wire (∅ 3.8 mm). Increased Zn content causes increases in ultimate tensile strength, yield strength and hardness (Strzępek et al., 2019). Situmorang et al. fabricated Cu with various Zn additions (10, 20, 38, and 45 wt.%) and found that the higher the Zn composition, the higher the antibacterial properties (Situmorang et al., 2019). Iqbal et al. melted Cu28.7Zn using a furnace and cast to investigate hardness and morphology (Iqbal et al., 2021). Shahriyari et al. added Zn (5, 15, 20, and 30 wt.%), increasing the hardness due to the alloy's rise in the Zn content

(Shahriyari et al., 2022). Akhyar et al. melted Cu28.7Zn using a gas furnace and cast to investigate the tensile strength (Akhyar et al., 2023). Morath et al. have created Zn0.8Cu and Zn1.5Cu using casting methods to investigate the biological aspect of arterial implants (Morath et al., 2024). Azizian et al. have added Cu with compositions 1, 2, and 5 wt.% to CuZn alloy by melting in the induction furnace to investigate microstructure, mechanical properties, and cytotoxicity for cardiovascular application (Azizian et al., 2024). Generally, a CuZn alloy with a Zn composition of less than 37 wt.% would produce a single alpha phase with an FCC crystal structure (Clement & Auger, 2023; Mousavi et al., 2020).

3. Research Methods

3.1 Material Preparation

Cu ingot (98.798 %) and Zn powder (99 %) were melted and cast with the alloy composition CuxZn (x=0, 6, 9, and 12 wt.%, namely as Cu, Cu6Zn, Cu9Zn, and Cu12Zn, respectively) and then confirmed the formed alloy using XRF (Table 1). Before melting was conducted, the ingot and the apparatus, such as the crucible, were cleaned using water to avoid impurities and then dried. The Cu ingot was first filled into a silicon carbide crucible (3kg) and then inserted into a muffle furnace. Melting was carried out in a crucible at 1100 °C under atmospheric pressure. After the Cu has melted, remove it from the muffle furnace, mix it with Zn powder, stir it manually, and pour it into a permanent mold. For comparison, Cu ingot was melted and poured into a permanent mold without Zn addition. The as-cast ingots were cut for further characterization, such as XRD, hardness, electrochemical measurement, and antibacterial activity observation.

Table 1 – Chemical composition of various casting samples.

Sample	Element (wt.%)					
	Cu	Zn	Al	Si	P	Fe
Cu	98.798	-	0.135	0.444	0.384	0.238
Cu6Zn	92.308	6.384	0.135	0.444	0.384	0.345
Cu9Zn	89.228	9.497	0.135	0.444	0.384	0.312
Cu12Zn	87.075	11.557	0.135	0.444	0.384	0.405

3.2 XRD Measurement

XRD was measured using the PANalytical (Cu Kα1 λ=1.5405980) apparatus. XRD was scanned from 20 to 100◦, using step size 0.0217◦. The Highscore software was used to refine and collect peak, phase and crystallographic parameters of as-cast samples. By using that software, full width at half maximum (FWHM) are also found. FWHM data is used to calculate crystallite size.

3.3 Hardness Measurement

Before testing, samples with 20×20×6 mm dimensions were polished using silicon carbide up to #3000 grit. Afterward, the polished sample was cleaned using water, followed by alcohol, and then dried using drier equipment. The hardness test was conducted using the Vickers method. An FV-300e hardness test was performed on top of various samples using 1 kg of load. Ten repeatable measurements were conducted.

3.4. Electrochemical Measurement

Two electrochemical measurements were conducted in the present research, such as open circuit potential (OCP) and Linear sweep voltammetry (LSV), using Digi-Ivy (DY2311) potentiostat in 0.9 % NaCl at room temperature. OCP was scanned until 1200 s using a sampling scan rate of 0.02 s, while LSV was conducted using a scan rate of 1 mV/s. Cu/CuZn samples are used as the working electrode, platinum wire as the counter electrode, and Ag/AgCl as the reference electrode. LSV data was examined using the Tafel extrapolation method to see corrosion potential (Ecorr) and current density (icorr). The corrosion rate could be found by inserting icorr in the following equation (Soegijono et al., 2020).

$$Corrosion\ rate\ (mmpy) = C\frac{M \times icorr}{\rho \times n} \quad (1)$$

Where C is corrosion constant (3.27 mmpy), M is atomic weight (g/mol), ρ is material density (g/cm^3), and n is the number of electrons involved.

3.5 Antibacterial Activity Observation

The sample dimension used for antibacterial activity is 20×20×6 mm. Before testing, samples were polished using silicon carbide up to #3000 grit. The experimental procedure for antibacterial activity is similar to that of the previous report (Syamsuir et al., 2023). Moreover, the recent study uses *Staphylococcus aureus* ATCC 25923 for Direct contact kill assay (24 hours) and Fluid contact assay (8 hours). In comparison, *Escherichia coli* 25922 was also used in the present study. Afterward, documentation was captured using a digital camera. In addition, 24-hour post-contact observation and Fluid contact test were also captured using a digital camera.

4. Results and Discussions

4.1 XRD

The diffraction pattern of Cu/CuZn with (111), (200), (311), and (222) planes can be seen in Figure 1. The four diffraction patterns match the alpha phase, which is shown to align with another study (Heidarzadeh et al., 2022). The acquired XRD data was then analyzed using Highscore software, and the parameters are listed in Table 2. All samples had a face-centered cubic (FCC) crystal structure, indicating that the Cu and Zn atoms dissolve into one another. According to Jinlong et al., the FCC quantity of surface energy is (111)>(001) >(110), and the FCC sample with the (111) plane has the lowest corrosion rate (Jinlong et al., 2016). Moreover, the FCC sample with the preferred orientation of the (111) plane has the highest surface atomic density (Soegijono et al., 2020).

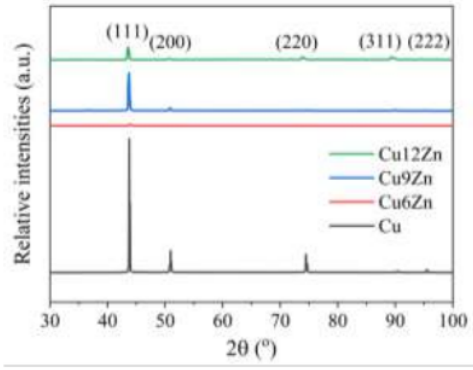

Fig. 1. XRD of various casting samples.

Table 2 - Crystallographic parameters of various casting samples.

Parameter	Sample			
	Cu	Cu6Zn	Cu9Zn	Cu12Zn
Crystal structure	FCC			
Lattice constant a = b = c (Å)	2.964	8.929	2.981	2.964
Cell volume (Å^3)	26.03	90	26.49	26.05
d-spacing (Å)	1.69	1.18	1.69	2.07
Crystallite Size (nm)	227.20	109.95	204.95	316.26
Micro strain	0.37	0.53	0.16	0.32

Presenting Zn in the alloy reduces crystallite size from 227.20 to 109.95 nm and increases Zn content from 6 to 12 wt.%, leading to an increase in crystallite size from 109.95 to 316.26 nm.

This behavior is similar to Özdemir and Karahan's study that showed Zn in the alloy leads to decreased crystallite size, and an increase in Zn content in the alloy leads to increased crystallite size (Özdemir & Karahan, 2014). Moreover, the microstrains of the as-cast sample are independent of Zn content, which perfectly agrees with Karahan and Özdemir's study ((Karahan & Özdemir, 2014). The smallest microstrain is seen in the Cu9Zn sample.

4.2 Hardness

Figure 2 shows the average hardness of various casting samples. Nikhil et al. have found that pure Cu has a hardness of 140 HV when treated at 400 and 600 °C and then held for two hours, followed by quenching in tap water, resulting in a hardness of 100 and 60 HV (Nikhil et al., 2021). The higher heat treatment temperatures led to a decrease in the hardness of the pure Cu. Therefore, the hardness of Cu may vary depending on heat treatment. In the present study, Cu re-casting has a hardness of 74.54 HV.

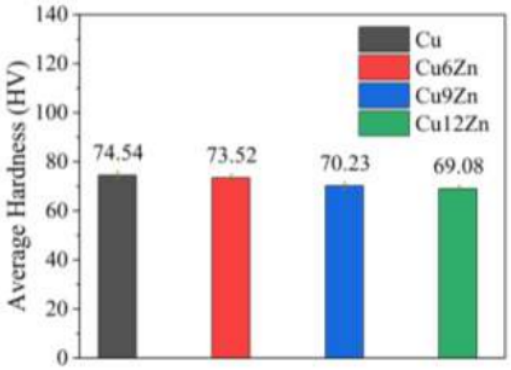

Fig. 2. Average hardness of various casting samples.

According to Figure 2, it can be seen that an increase in Zn content led to a decrease in the hardness. Another research study found that Cu (as-cast) has a hardness of around 100 HV, while Cu15 Zn (as-cast) has a hardness of 75 HV (Ezequiel et al., 2024). Nnakwo et al. also found that increased Zn content in the Cu alloy leads to decreased hardness due to increased in grain size and solid solution region (Nnakwo et al., 2021). According to a study by Qu et al. and García-Mintegui et al., pure Zn hardness is between 41-42 HV (García-Mintegui et al., 2021; Qu et al., 2020). Therefore, it could be concluded that Zn in the alloy leads to decreased hardness due to Zn hardness less than Cu.

Several researchers correlated measured hardness to crystallite size (Augustin et al., 2016; Syamsuir et al., 2023). Augustin et al. have found an increase in Cu's crystallite size, promoting a decrease in scratch and micro-hardness (Augustin et al., 2016). Syamsuir et al. found a decrease in Cu's crystallite size, leading to an increase in hardness (Syamsuir et al., 2023). Comparing Table 2 with Figure 2, it can be seen that an increase in the Zn content led to an increase in crystallite size and a decrease in the hardness. On the contrary, while as-cast samples do not form an alloy (Cu), the resulting hardness is not aligned with the crystallite size. It seems that it cannot compare the crystallite size were found with measured hardness between alloy (CuZn) and un-alloy (Cu) material.

Several transportation sectors, such as ambulance equipment, are made from Al alloy (Blanco et al., 2022; Vandersluis et al., 2020). According to Hajizadeh et al., Al alloy hardness is between 32-52 HV (Hajizadeh et al., 2017). Therefore, all specimens have hardness still higher than Al alloy.

4.3 OCP

Figure 3 shows the OCP measurement result of various casting samples in 0.9 % NaCl at room temperature. Generally, increased Zn content in the alloy promoted more negative potential,

which perfectly agrees with the Cocco et al. study (Cocco et al., 2016). Dridi et al. have found that E_{OCP} CuZn30 and CuZn39 are -0.578 and -0.604 V/MSE at 3 % NaCl, which means an increase in the Zn promoted to more negative potential (Dridi et al., 2020). Cu, Cu6Zn, Cu9Zn, and Cu12Zn samples have E_{OCP} potential at 1200 s measurement -0.014, -0.023, -0.027, and -0.032 V vs Ag/AgCl, respectively.

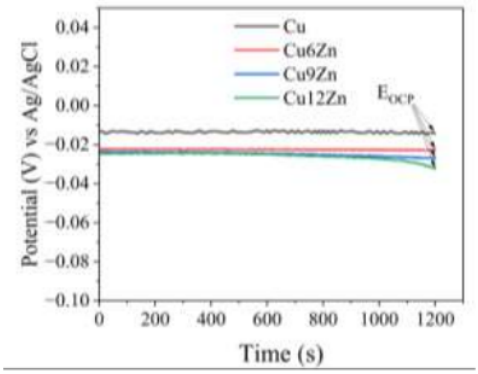

Fig. 3. OCP measurement of various casting samples.

According to Figure 3, Cu, Cu6Zn, and Cu9Zn samples are steady at initial measurements until 1200 s, indicating that the protective layer formed has good protection. In contrast, the Cu12Zn sample is steady at initial measurements until 600 s, then moves in a more negative direction. These phenomena indicated that the formed protective layer had initially dissolved at 600 s; therefore, the measurement continuously moved forward in a negative direction until the measurement reached 1200 s.

4.4 LSV

Eccrine sweat and saline-infused for humans are nearly 0.9 % of NaCl (Bond & Lieu, 2014; Tayyab et al., 2021). Therefore, LSV measurement was conducted in 0.9 % NaCl at room temperature. Luo et al. found Cu_2O crystalline growth on the Cu surface when exposed to 0.9 % NaCl, while when exposed to pure water, Cu_2O crystalline was not seen (Luo et al., 2020). Commonly, Cu_2O crystallines are formed, which is preceded by the formation of CuCl when the specimen is tested in a chloride solution. Moreover, Zhang et al., in their study, found ZnO and $Zn_5Cl_2(OH)_8{\cdot}H_2O$ as corrosion products on top of Cu40Zn surfaces in a chloride environment (Zhang et al., 2016). The reaction of Cu in chloride solution is as follows (Milošev et al., 2024).

$$O_2 + 2H_2O + 4e^- \rightarrow 4OH^- \quad (2)$$
$$Cu + 2Cl^- \leftrightarrows CuCl_2^- + e^- \quad (3)$$
$$Cu + Cl^- \leftrightarrows CuCl + e^- \quad (4)$$
$$CuCl + Cl^- \leftrightarrows CuCl_2^- \quad (5)$$
$$Cu \leftrightarrows Cu^+ + e^- \quad (6)$$
$$Cu^+ + 2Cl^- \leftrightarrows CuCl_2^- \quad (7)$$

The reaction of Zn in chloride solution is as follows (Milošev et al., 2024).

$$Zn \longrightarrow Zn^{2+} + 2e^- \quad (8)$$
$$Zn^{2+} + 2OH^- \longrightarrow Zn(OH)_2 \longrightarrow ZnO + H_2O \quad (9)$$
$$5Zn^{2+} + 8OH^- + 2Cl^- + H_2O \longrightarrow Zn_5(OH)_8Cl_2 \cdot H_2O \quad (10)$$

LSV measurement results in 0.9 % NaCl can be seen in Figure 4.

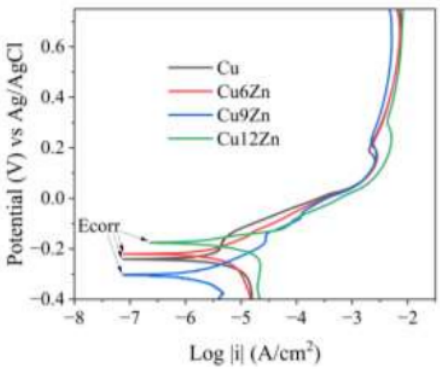

Fig. 4. LSV scans result of various casting samples.

According to Figure 4, corrosion Ecorr and icorr can be found using the Tafel extrapolation method. Moreover, the corrosion rate could be calculated by inserting icorr into expression (1). Table 3 presented Ecorr, icorr, and the corrosion rate of various casting samples. It appears Ecorr is independent of Zn addition; however, Zn is dependent on icorr and corrosion rate (except for the Cu12Zn sample). This behavior is probably due to a protective layer that was formed. Compared to the OCP result, it can be seen that the Cu12Zn sample continuously moves forward in a negative direction from 600 until 1200 s of measurement. Therefore, that sample has a higher icorr and corrosion rate.

Table 3 - Corrosion parameters of various casting samples.

Sample name	Ecorr (V) vs Ag/AgCl	Icorr (A/cm²)	Corrosion rate (mmpy)
Cu	-0.241	4.42×10^{-6}	5.13×10^{-2}
Cu6Zn	-0.220	3.33×10^{-6}	3.86×10^{-2}
Cu9Zn	-0.304	2.15×10^{-6}	2.49×10^{-2}
Cu12Zn	-0.175	6.19×10^{-6}	7.18×10^{-2}

Qu et al. have found that an increase in Zn content led to an increase in corrosion resistance, which perfectly agrees with the present study (except for Cu12Zn) (Qu et al., 2020). Milošev et al. investigated Cu, Cu10Zn, Cu40Zn, and Zn in 3 % NaCl and found icorr after stabilized at 1 hour around 1.573, 1.456, and 2.114, and 5.21 μA/cm² respectively (Milošev et al., 2024). According to equation (1), icorr strongly influences the corrosion rate. The more icorr, the higher the corrosion rate. Moreover, a limitation in Zn content in the Cu alloy could influence the corrosion resistance. Presenting the Zn content ≤ 11 wt.% in the alloy could enhance the corrosion resistance; however, Zn of more than 10 wt.% could decrease corrosion resistance (Milošev et al., 2024).

According to Table 2, the Cu9Zn sample has the lowest microstrain than others. The measured microstrain could be associated with the sample's crystal defect (Soegijono et al., 2020). Based on Table 2, the Cu9Zn sample has the lowest microstrain, which confirms that the sample has the lowest corrosion rate. Moreover, the FCC sample with the preferred orientation of the (111) plane could offer a lower corrosion rate due to the highest surface atomic density (Jinlong et al., 2016; Soegijono et al., 2020). Compared to other samples, the Cu9Zn sample has the higher preferred orientation of the (111) plane. Even though the (111) plane of the Cu sample is the highest. Unfortunately, the (220) and (200) planes are still present and relatively high.

4.5 Antibacterial Activity

Figure 5 shows the direct contact kill of *Staphylococcus aureus* and *Escherichia coli* after 24 hours of incubation**.** The present study focused on *Staphylococcus aureus*, but *Escherichia coli* was also used for comparison. There is no diffusion in the sample; therefore, the inhibition zone could not be seen.

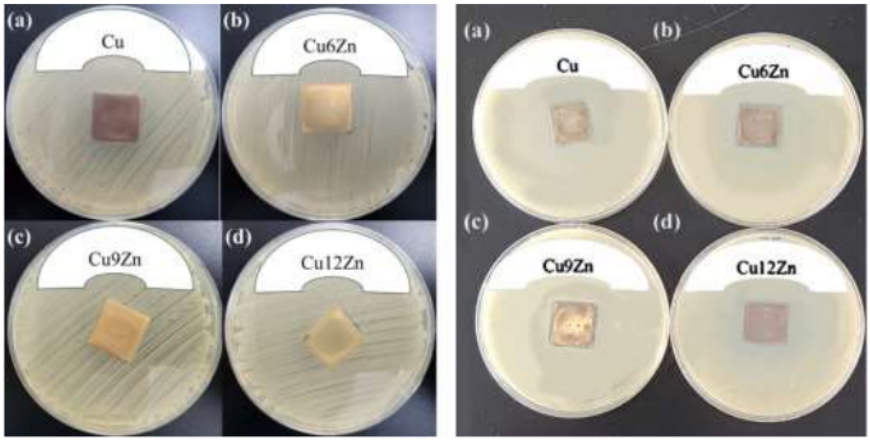

Fig. 5. Antibacterial activity test using *Staphylococcus aureus* (left) and *Escherichia coli* (right) (a) Cu, (b) Cu6Zn, (c) Cu9Zn, and (d) Cu12Zn.

Antibacterial activity after 24 hours of post-contact with various casting samples using *Staphylococcus aureus* and *Escherichia coli* can be seen in Figure 6. The removed sample places remain clear (with no regrowth) from bacterial activity. The antibacterial behavior was significantly influenced by Cu or Zn ions (Qu et al., 2020). Villapún et al. found that releasing Cu ions leads to the highest killing activity of *Staphylococcus aureus* (Villapún et al., 2016). Excess in the Cu ion could be bacteriostatic (Sabbouh et al., 2023). Moreover, Cu ions could be adsorbed on the cytoplasmic membrane surfaces, then penetrate the bacteria, react with sulfhydryl groups and cause the cell to die (Zeng et al., 2022). Furthermore, Cu ions could form hydroxyl groups in the presence of oxygen in nature, which could destroy cell membranes (Dou et al., 2022). Hutchings et al. stated that Zn^{2+} successfully inhibits the growth of *S. epidermidis* (Hutchings et al., 2021). This behavior is associated with the generation of reactive oxygen or the formation of (Zhang et al., 2021).

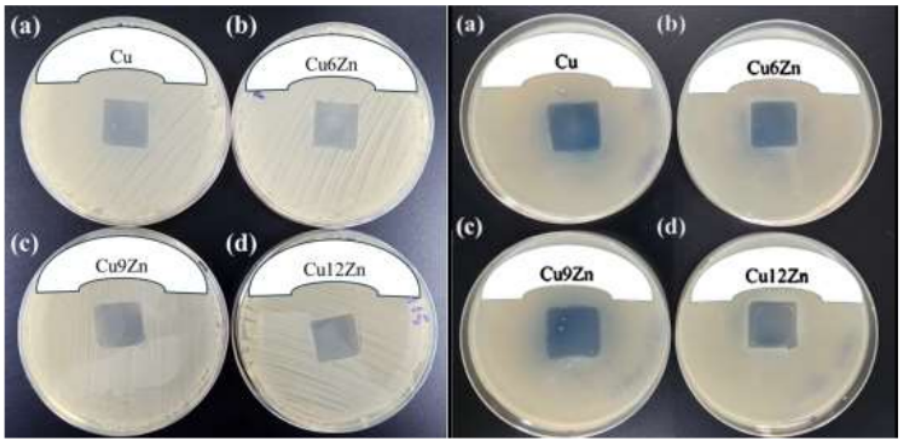

Fig. 6. Antibacterial activity after 24 hours of post-contact (regrowth assessment) towards *Staphylococcus aureus* (left) and *Escherichia coli* (right) (a) Cu, (b) Cu6Zn, (c) Cu9Zn, and (d) Cu12Zn

Figure 7 shows the fluid contact test of *Staphylococcus aureus* and *Escherichia coli*. The orientation of the test materials is mapped within the yellow box. For the Cu6Zn sample, *Escherichia coli* was killed on the 3rd hour. However, there is no significant reduction within the

fluid because there are no diffusible materials. Also, there is no visible growth after 3rd hour for the fluid in contact with the metal.

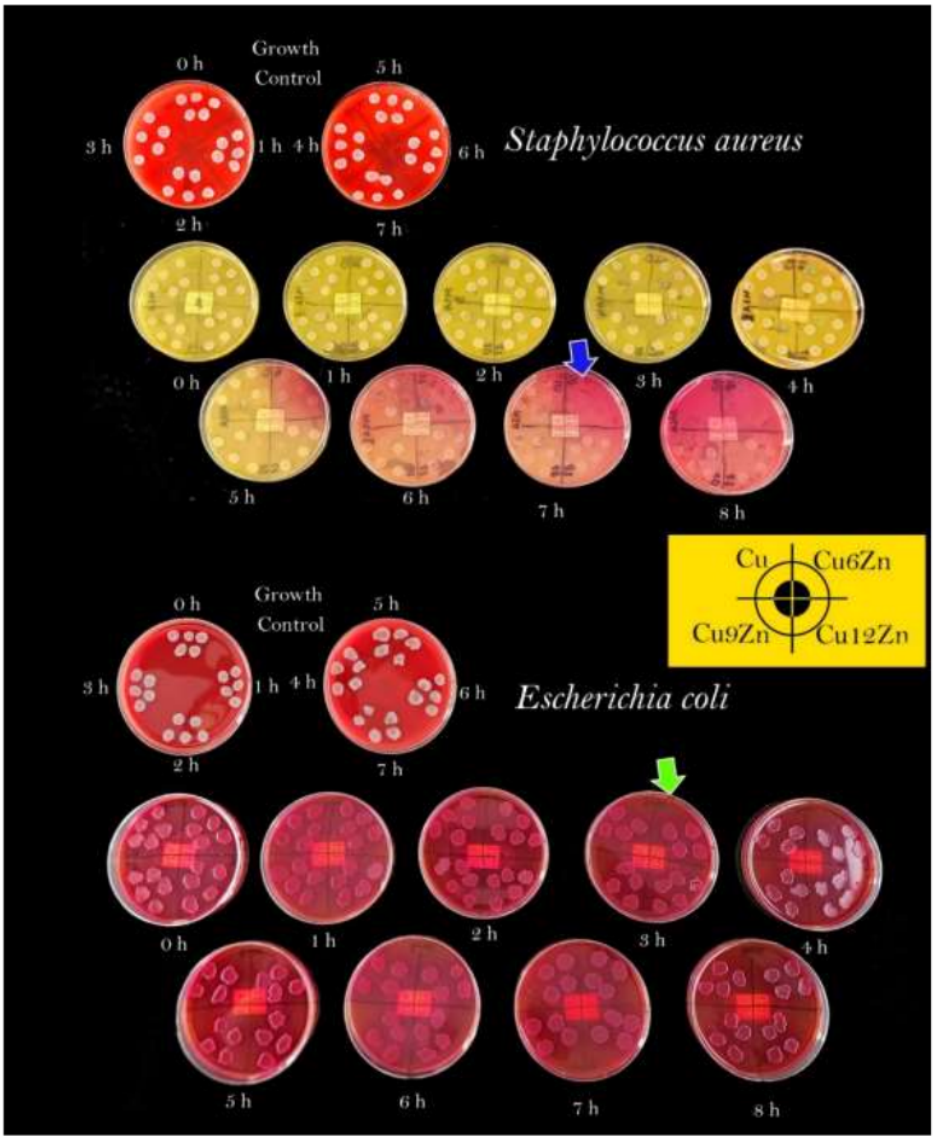

Fig. 7. Fluid contact test of *Staphylococcus aureus* and *Escherichia coli*

Moreover, it should be noted that the reduction of the colony is significant in the 7th hour for *Staphylococcus aureus* (blue arrow), but for *Escherichia coli*, the inhibition of *Escherichia coli* growth is shown within the 3rd hour of contact (green arrow), for Cu6Zn sample. The reduction of colonies is significant on the surface of the metal. While on the remaining fluid, the reduction is insignificant until 8 hours. This behavior is because *Staphylococcus aureus* and *Escherichia coli* have different membrane structures and thick cell walls, therefore could inhibit ion exchange and restrain the antibacterial effect of Cu and or Zn ions (Di et al., 2022). Cu killing is more effective in Gram-negative bacteria (e.g., *Escherichia coli*) because peptidoglycan affects the cell's susceptibility. The thicker the peptidoglycan layer, the harder it became for the Cu ions

to reach the membrane (Soltani et al., 2020; Xhafa et al., 2023). Therefore, *Escherichia coli* was killed in the 3rd hour. Another reason Cu6Zn has better antibacterial performance than others is probably due to its smaller crystallite size. Researchers found that smaller crystallite sizes promote the enhancement of antibacterial effects (Syamsuir et al., 2023). This behavior is attributed to an increase in surface area due to the crystallite size (Sangeetha et al., 2015). The Cu6Zn sample could be used as an alternative material for medical equipment in ambulances.

5. Conclusion

CuZn has been successfully fabricated. XRD confirmed that CuZn alloy has a single alpha phase with an FCC crystal structure. The rise of the Zn content in the alloy led to a decrease in the hardness due to an increase in crystallite size and led to a shift to more negative OCP potential at 1200 s measurement. Moreover, the rise of the Zn content to 9 wt.% decreased the corrosion rate. It appears there is a limitation in Zn content in the copper alloy that influences the corrosion rate, as shown when Zn content around 12 wt. % is promoted to increase the corrosion rate. Antibacterial activity observation found that all samples had no diffusion. Moreover, 24-hour post-contact observation found that sample places removed from the sample remained clear of bacteria. The Cu6Zn has better antibacterial performance than others due to the smallest crystallite size. According to the fluid contact test, the reduction of the colony of *Staphylococcus aureus* is significant in the 7th hour. The inhibition of *Escherichia coli* growth is also shown within the 3rd hour of contact. This behavior is because *Staphylococcus aureus* and *Escherichia coli* have different membrane structures and thick cell walls, therefore, could inhibit ion exchange and restrain the antibacterial effect of Cu and or Zn ions.

Acknowledgement

This research is under financial support from the Ministry of Education, Culture, Research and Technology Indonesia with contract number 832/LL3/AL.04/2024 and 171/A/LPPM-P/USAKTI/VI/2024.

References

Abed, K. M., & Dawood, N. M. (2022). Impacts of Tin and Germanium on Corrosion and Erosion-Corrosion Behavior of 60Cu-40Zn alloys. *AIP Conference Proceedings*, *2660*, 020131. https://doi.org/10.1063/5.0108474

Akhyar, Iqbal, Ali, N., & Husin, H. (2023). Effect of variations in pouring temperature on tensile strength of CuZn cast alloys. *Materials Letters: X*, *17*, 100182. https://doi.org/10.1016/j.mlblux.2023.100182

Augustin, A., Huilgol, P., Udupa, K. R., & Bhat K, U. (2016). Effect of current density during electrodeposition on microstructure and hardness of textured Cu coating in the application of antimicrobial Al touch surface. *Journal of the Mechanical Behavior of Biomedical Materials*, *63*, 352–360. https://doi.org/10.1016/j.jmbbm.2016.07.013

Azizian, F., Naffakh-Moosavy, H., & Bagheri, F. (2024). The role of Cu addition in the metallurgical features, mechanical properties, and cytocompatibility of cardiovascular stents biodegradable Zn-based alloy. *Intermetallics*, *164*, 108106. https://doi.org/10.1016/j.intermet.2023.108106

Baker, L. B., & Wolfe, A. S. (2020). Physiological mechanisms determining eccrine sweat composition. *European Journal of Applied Physiology*, *120*(4), 719–752. https://doi.org/10.1007/s00421-020-04323-7

Bhavsar, V., & Bali, S. C. (2023). Effect of Compressed Natural Gas (CNG) on corrosion behaviour of brass valve of CNG cylinder. *Engineering Failure Analysis*, *149*, 107268. https://doi.org/10.1016/j.engfailanal.2023.107268

Blanco, D., Mar, E., & Mar, R. (2022). Titanium Alloys Applied to the Transport Sector : A Review. *Metals*, *12*(9), 1–21. https://doi.org/10.3390/met12010009

Bond, J. W., & Lieu, E. (2014). Electrochemical behaviour of brass in chloride solution concentrations found in eccrine fingerprint sweat. *Applied Surface Science*, *313*, 455–461. https://doi.org/10.1016/j.apsusc.2014.06.005

Chen, L., Ma, R., Dong, J., Chen, S., Li, C., Ma, C., Bian, G., & Wang, C. (2024). A multi-ion

transport model of Cu-Zn-Fe trimetallic couple in near-neutral NaCl solution. *Corrosion Science*, *239*, 112414. https://doi.org/10.1016/j.corsci.2024.112414

Clement, A., & Auger, T. (2023). An EAM potential for α-brass copper-zinc alloys: application to plasticity and fracture. *Modelling and Simulation in Materials Science and Engineering*, *31*(1), 015004. https://doi.org/10.1088/1361-651X/aca4ec

Cocco, F., Fantauzzi, M., Elsener, B., & Rossi, A. (2016). Dissolution of brass alloys naturally aged in neutral solutions-an electrochemical and surface analytical study. *RSC Advances*, *6*(93), 90654–90665. https://doi.org/10.1039/c6ra18200c

Di, T., Xu, Y., Liu, D., & Sun, X. (2022). Microstructure, Mechanical Performance and Anti-Bacterial Activity of Degradable Zn-Cu-Ag Alloy. *Metals*, *12*(9), 1–13. https://doi.org/10.3390/met12091444

Dou, X., Chen, Y., & Shi, H. (2022). CuBi2O4/BiOBr composites promoted PMS activation for the degradation of tetracycline: S-scheme mechanism boosted Cu2+/Cu+ cycle. *Chemical Engineering Journal*, *431*(P2), 134054. https://doi.org/10.1016/j.cej.2021.134054

Dridi, A., Dhouibi, L., Hihn, J. Y., Berçot, P., Rezrazi, E. M., Sassi, W., & Rouge, N. (2020). Analytical Study of CuZn 30 and CuZn 39 Brass Surfaces in 3% NaCl Solution Under Polarization. *Chemistry Africa*, *3*(3), 735–747. https://doi.org/10.1007/s42250-020-00182-z

Du, M., Zhao, W., Ma, R., Xu, H., Zhu, Y., Shan, C., Liu, K., Zhuang, J., & Jiao, Z. (2021). Visible-light-driven photocatalytic inactivation of S. aureus in aqueous environment by hydrophilic zinc oxide (ZnO) nanoparticles based on the interfacial electron transfer in S. aureus/ZnO composites. *Journal of Hazardous Materials*, *418*, 126013 Contents. https://doi.org/10.1016/j.jhazmat.2021.126013

Ezequiel, M., Proriol Serre, I., Auger, T., Héripré, E., Hadjem-Hamouche, Z., & Perriere, L. (2024). The liquid metal embrittlement of a reactive system at room temperature: α-brasses in contact with the liquid eutectic Ga-In. *Engineering Failure Analysis*, *164*, 108694. https://doi.org/10.1016/j.engfailanal.2024.108694

Gao, P., Ren, Y., Qian, S., He, Y., & Shen, D. (2021). Evolution of microstructure and electrochemical corrosion behavior of CuZn-based alloys induced by cold rolling. *Journal of Materials Research and Technology*, *15*, 360–368. https://doi.org/10.1016/j.jmrt.2021.08.035

García-Mintegui, C., Córdoba, L. C., Buxadera-Palomero, J., Marquina, A., Jiménez-Piqué, E., Ginebra, M. P., Cortina, J. L., & Pegueroles, M. (2021). Zn-Mg and Zn-Cu alloys for stenting applications: From nanoscale mechanical characterization to in vitro degradation and biocompatibility. *Bioactive Materials*, *6*(12), 4430–4446. https://doi.org/10.1016/j.bioactmat.2021.04.015

Hajizadeh, K., Ejtemaei, S., & Eghbali, B. (2017). Microstructure, hardness homogeneity, and tensile properties of 1050 aluminum processed by constrained groove pressing. *Applied Physics A: Materials Science and Processing*, *123*(8), 1–9. https://doi.org/10.1007/s00339-017-1123-y

Heidarzadeh, A., Javidani, M., & St-Georges, L. (2022). Crystallographic Orientation Relationship between α and β Phases during Non-Equilibrium Heat Treatment of Cu-37 wt. % Zn Alloy. *Crystals*, *12*(1), 97. https://doi.org/10.3390/cryst12010097

Hendrawan, C. N., Setyani, A., Pertiwi, D. R. K., & Sofyan, B. T. (2021). Effect of 9wt% Mn addition on cold rolling and annealing behaviour of Cu-31Zn alloy. *Materials Today: Proceedings*, *46*, 3346–3351. https://doi.org/10.1016/j.matpr.2020.11.476

Huang, S. J., Li, C., Feng, J. H., Selvaraju, S., & Subramani, M. (2024). Mechanical and Corrosion Tests for Magnesium–Zinc/Ti-6Al-4V Composites by Gravity Casting. *Materials*, *17*(8), 1836. https://doi.org/10.3390/ma17081836

Hutchings, C., Yair, Z. P., Reifen, R., & Shemesh, M. (2021). Antimicrobial effect of zn2+ ions governs the microbial quality of donor human milk. *Foods*, *10*(3), 1–12. https://doi.org/10.3390/foods10030637

Iqbal, Ali, N., Husin, H., Akhyar, Khairil, & Farhan, A. (2021). Differences in Pour Temperature Affect Hardness Properties of CuZn Brass Alloy through Metal Casting. *IOP Conference Series: Materials Science and Engineering*, *1082*(1), 012001.

https://doi.org/10.1088/1757-899x/1082/1/012001

Jinlong, L., Tongxiang, L., & Chen, W. (2016). Effect of electrodeposition temperature on grain orientation and corrosion resistance of nanocrystalline pure nickel. *Journal of Solid State Chemistry*, *240*, 109–114. https://doi.org/10.1016/j.jssc.2016.05.025

Karahan, I. H., & Özdemir, R. (2014). Effect of Cu concentration on the formation of Cu 1-x Zn x shape memory alloy thin films. *Applied Surface Science*, *318*, 100–104. https://doi.org/10.1016/j.apsusc.2014.01.119

Liu, P., Hu, J. ying, Li, H. xue, Sun, S. yu, & Zhang, Y. bin. (2020). Effect of heat treatment on microstructure, hardness and corrosion resistance of 7075 Al alloys fabricated by SLM. *Journal of Manufacturing Processes*, *60*, 578–585. https://doi.org/10.1016/j.jmapro.2020.10.071

Luo, J., Hein, C., Pierson, J. F., & Mücklich, F. (2020). Sodium chloride assists copper release, enhances antibacterial efficiency, and introduces atmospheric corrosion on copper surface. *Surfaces and Interfaces*, *20*, 100630. https://doi.org/10.1016/j.surfin.2020.100630

Milošev, I., Taheri, P., Kapun, B., Kozlica, D. K., Mol, A., & Kokalj, A. (2024). The effect of molecular structure of imidazole-based compounds on corrosion inhibition of Cu, Zn, and Cu-Zn alloys. *Corrosion Science*, 127870. https://doi.org/10.1016/j.corsci.2024.112328

Morath, L., Rahim, S. A., Baker, C., Anderson, D., Hinds, M., Sikora-Jasinska, M., Oujiri, L., Leyssens, L., Kerckhofs, G., Pyka, G., Oliver, A. A., Drelich, J. W., & Goldman, J. (2024). The biological effects of copper alloying in Zn-based biodegradable arterial implants. *Biomaterials Advances*, *November*, 124658. https://doi.org/10.1016/j.bioadv.2024.214112

Mousavi, S. E., Sonboli, A., Naghshehkesh, N., Meratian, M., Salehi, A., & Sanayei, M. (2020). Different behavior of alpha and beta phases in a Low Stacking Fault Energy copper alloy under severe plastic deformation. *Materials Science and Engineering: A*, *788*, 139550. https://doi.org/10.1016/j.msea.2020.139550

Nikhil, Singh, M. K., Ji, G., & Prakash, R. (2021). Investigation on the effects of cooling rate on surface Texture, corrosion behaviour and hardness of pure copper. *Materials Today: Proceedings*, *47*(19), 6693–6695. https://doi.org/10.1016/j.matpr.2021.05.115

Nnakwo, K. C., Osakwe, F. O., Ugwuanyi, B. C., Oghenekowho, P. A., Okeke, I. U., & Maduka, E. A. (2021). Grain characteristics, electrical conductivity, and hardness of Zn-doped Cu–3Si alloys system. *SN Applied Sciences*, *3*(11), 829. https://doi.org/10.1007/s42452-021-04784-1

Nuryadi, N., Sudarsono, B., & Asistyasari, A. (2020). Effect of Moisture Content of Green Sand on The Casting Defects. *Journal of Applied Engineering and Technological Science*, *4*(1), 586–598.

Özdemir, R., & Karahan, I. H. (2014). Electrodeposition and properties of Zn, Cu, and Cu 1-x Zn x thin films. *Applied Surface Science*, *318*, 314–318. https://doi.org/10.1016/j.apsusc.2014.06.188

Pietrocola, G., Campoccia, D., Motta, C., Montanaro, L., Arciola, C. R., & Speziale, P. (2022). Colonization and Infection of Indwelling Medical Devices by Staphylococcus aureus with an Emphasis on Orthopedic Implants. *International Journal of Molecular Sciences*, *23*(11), 5958. https://doi.org/10.3390/ijms23115958

Qu, X., Yang, H., Jia, B., Yu, Z., Zheng, Y., & Dai, K. (2020). Biodegradable Zn–Cu alloys show antibacterial activity against MRSA bone infection by inhibiting pathogen adhesion and biofilm formation. *Acta Biomaterialia*, *117*, 400–417. https://doi.org/10.1016/j.actbio.2020.09.041

Riaz, M., Najam, M., Imtiaz, H., Bashir, F., & Hussain, T. (2024). Structural and biological analysis of Zn–Cu based biodegradable alloys for orthopedic application. *Materials Chemistry and Physics*, *312*, 128618. https://doi.org/10.1016/j.matchemphys.2023.128618

Sabbouh, M., Nikitina, A., Rogacheva, E., Nebalueva, A., Shilovskikh, V., Sadovnichii, R., Koroleva, A., Nikolaev, K., Kraeva, L., Ulasevich, S., & Skorb, E. (2023). Sonochemical fabrication of gradient antibacterial materials based on Cu-Zn alloy. *Ultrasonics Sonochemistry*, *92*, 106247. https://doi.org/10.1016/j.ultsonch.2022.106247

Sangeetha, R., Muthukumaran, S., & Ashokkumar, M. (2015). Structural, optical, dielectric and antibacterial studies of Mn doped Zn0.96Cu0.04O nanoparticles. *Spectrochimica Acta* -

Part A: Molecular and Biomolecular Spectroscopy, *144*, 1–7. https://doi.org/10.1016/j.saa.2015.02.056

Shahriyari, F., Shaeri, M. H., Dashti, A., Zarei, Z., Noghani, M. T., Cho, J. H., & Djavanroodi, F. (2022). Evolution of mechanical properties, microstructure and texture and of various brass alloys processed by multi-directional forging. *Materials Science and Engineering: A*, *831*, 142149. https://doi.org/10.1016/j.msea.2021.142149

Situmorang, E. M. H., Henniwuriyama, V., & Soegijono, B. (2019). Oligodynamic Cu-Zn composite fabricated by powder metallurgy method. *Journal of Physics: Conference Series*, *1191*(1). https://doi.org/10.1088/1742-6596/1191/1/012044

Soegijono, B., Susetyo, F. B., Yusmaniar, & Fajrah, M. C. (2020). Electrodeposition of paramagnetic copper film under magnetic field on paramagnetic aluminum alloy substrates. *E-Journal of Surface Science and Nanotechnology*, *18*, 281–288. https://doi.org/10.1380/EJSSNT.2020.281

Soltani, S., Akhbari, K., & White, J. (2020). Synthesis, crystal structure, magnetic, photoluminescence and antibacterial properties of dinuclear Copper(II) complex. *Journal of Molecular Structure*, *1214*, 128233. https://doi.org/10.1016/j.molstruc.2020.128233

Strzępek, P., Mamala, A., Zasadzińska, M., Franczak, K., & Jurkiewicz, B. (2019). Research on the drawing process of Cu and CuZn wires obtained in the cryogenic conditions. *Cryogenics*, *100*, 11–17. https://doi.org/10.1016/j.cryogenics.2019.03.007

Syamsuir, Susetyo, F. B., Soegijono, B., Yudanto, S. D., Basori, Ajiriyanto, M. K., Edbert, D., Situmorang, E. U. M., Nanto, D., & Rosyidan, C. (2023). Rotating-Magnetic-Field-Assisted Electrodeposition of Copper for Ambulance Medical Equipment. *Automotive Experiences*, *6*(2), 290–302. https://doi.org/10.31603/ae.9067

Tajik, S., Najar-Peerayeh, S., & Bakhshi, B. (2020). Hospital clones of Panton-Valentine leukocidin-positive and methicillin-resistant Staphylococcus aureus circulating in the Tehran community. *Journal of Global Antimicrobial Resistance*, *22*, 177–181. https://doi.org/10.1016/j.jgar.2019.12.010

Tayyab, K. Bin, Farooq, A., Alvi, A. A., Nadeem, A. B., & Deen, K. M. (2021). Corrosion behavior of cold-rolled and post heat-treated 316L stainless steel in 0.9wt% NaCl solution. *International Journal of Minerals, Metallurgy and Materials*, *28*(3), 440–449. https://doi.org/10.1007/s12613-020-2054-8

Vandersluis, E., Machin, A., Perovic, D., & Ravindran, C. (2020). Failure Analysis of an Ambulance Cathode Ray Tube Monitor Bracket. *Journal of Failure Analysis and Prevention*, *20*(1), 23–33. https://doi.org/10.1007/s11668-020-00804-1

Viegas, C., Sousa, P., Dias, M., Caetano, L. A., Ribeiro, E., Carolino, E., Twarużek, M., Kosicki, R., & Viegas, S. (2021). Bioburden contamination and Staphylococcus aureus colonization associated with firefighter's ambulances. *Environmental Research*, *197*, 111125. https://doi.org/10.1016/j.envres.2021.111125

Villapún, V. M., Dover, L. G., Cross, A., & González, S. (2016). Antibacterial metallic touch surfaces. *Materials*, *9*(9), 1–23. https://doi.org/10.3390/ma9090736

Wang, X., Su, H., Xie, Y., Wang, J., Feng, C., Li, D., & Wu, T. (2023). Atmospheric corrosion of T2 copper and H62 brass exposed in an urban environment. *Materials Chemistry and Physics*, *299*, 127487. https://doi.org/10.1016/j.matchemphys.2023.127487

Widyastuti, Rochiem, R., Fellicia, D. M., Adrinanda, C. F. N., & Wibowo, A. P. (2023). Mechanical Properties, Microstructural, and Deep Drawing Formability Analysis on the Annealed CuZn35 Brass Alloy for Cartridge Application. *Key Engineering Materials*, *939*, 31–37. https://doi.org/10.4028/p-21x8y5

Xhafa, S., Olivieri, L., Di Nicola, C., Pettinari, R., Pettinari, C., Tombesi, A., & Marchetti, F. (2023). Copper and Zinc Metal–Organic Frameworks with Bipyrazole Linkers Display Strong Antibacterial Activity against Both Gram+ and Gram− Bacterial Strains. *Molecules*, *28*(16), 6160. https://doi.org/10.3390/molecules28166160

Yin, M. yang, Li, Z., Xiao, Z., Pang, Y., Li, Y. ping, & Shen, Z. yan. (2021). Corrosion behavior of Cu–Al–Mn–Zn–Zr shape memory alloy in NaCl solution. *Transactions of Nonferrous Metals Society of China (English Edition)*, *31*(4), 1012–1022. https://doi.org/10.1016/S1003-6326(21)65557-7

Zeng, J., Geng, X., Tang, Y., Xiong, Z. C., Zhu, Y. J., & Chen, X. (2022). Flexible photothermal biopaper comprising Cu2+-doped ultralong hydroxyapatite nanowires and black phosphorus nanosheets for accelerated healing of infected wound. *Chemical Engineering Journal*, *437*, 135347. https://doi.org/10.1016/j.cej.2022.135347

Zhang, E., Zhao, X., Hu, J., Wang, R., Fu, S., & Qin, G. (2021). Antibacterial metals and alloys for potential biomedical implants. *Bioactive Materials*, *6*(8), 2569–2612. https://doi.org/10.1016/j.bioactmat.2021.01.030

Zhang, X., Liu, X., Odnevall Wallinder, I., & Leygraf, C. (2016). The protective role of hydrozincite during initial corrosion of a Cu40Zn alloy in chloride-containing laboratory atmosphere. *Corrosion Science*, *103*, 20–29. https://doi.org/10.1016/j.corsci.2015.10.027

Ziat, Y., Hammi, M., Laghlimi, C., & Moutcine, A. (2020). Investment casting of leaded brass: Microstructure micro-hardness and corrosion protection by epoxy coating. *Materialia*, *12*, 100794 Contents. https://doi.org/10.1016/j.mtla.2020.100794

EFFECT OF ZINC ADDITION IN COPPER TO STRUCTURE, HARDNESS, CORROSION, AND ANTIBACTERIAL ACTIVITY

ORIGINALITY REPORT

20%	12%	11%	4%
SIMILARITY INDEX	INTERNET SOURCES	PUBLICATIONS	STUDENT PAPERS

MATCH ALL SOURCES (ONLY SELECTED SOURCE PRINTED)

1%

★ m.riunet.upv.es

Internet Source

Exclude quotes	Off	Exclude matches	Off
Exclude bibliography	Off		